SCIENTIFIC REPORTS

OPEN

SUBJECT AREAS:
BIOMARKERS
ENZYME MECHANISMS
MALARIA
VIRTUAL SCREENING

Received
28 March 2013

Accepted
6 August 2013

Published
26 August 2013

Correspondence and requests for materials should be addressed to H.S.Y. (hsyoon@ntu.edu.sg)

* These authors contributed equally to this work.

† Current address: Immunology Unit, Pasteur Institute of Dakar, BP 220 Dakar, Senegal.

Small molecule *Plasmodium* FKBP35 inhibitor as a potential antimalaria agent

Amaravadhi Harikishore*, Makhtar Niang*†, Sreekanth Rajan*, Peter Rainer Preiser & Ho Sup Yoon

School of Biological Science, Nanyang Technological University, 60 Nanyang Drive, Singapore 637665.

Malaria parasite strains have emerged to tolerate the therapeutic effects of the prophylactics and drugs presently available. This resistance now poses a serious challenge to researchers in the bid to overcome malaria parasitic infection. Recent studies have shown that FK520 and its analogs inhibit malaria parasites growth by binding to FK506 binding proteins (FKBPs) of the parasites. Structure based drug screening efforts based on three-dimensional structural information of FKBPs from *Plasmodium falciparum* led us to identify new chemical entities that bind to the parasite FKBP35 and inhibit its growth. Our experimental results verify that this novel compound (D44) modulate the PPIase activity of *Plasmodium* FKBP35 and demonstrate the stage-specific growth inhibition of *Plasmodium falciparum* strains. Here, we present the X-ray crystallographic structures of FK506 binding domains (FKBDs) of *Pf*FKBP35 and *Pv*FKBP35 in complex with the newly identified inhibitor providing molecular insights into its mode of action.

With an estimated 800,000 deaths annually, malaria is one of the most prevalent and dangerous infectious diseases currently afflicting the tropical and sub-tropical regions of India, Africa, Southeast Asia and South America[1,2]. Among the five *Plasmodium* species, *P. falciparum* and *P. vivax*, are the most virulent and chronic forms that cause malaria infection in humans triggering the lethal cerebral malaria and death. In recent years, these parasites have developed resistance to current therapeutics, of particular concern are recent reports showing the first appearance of artemisinin resistance in *P. falciparum* in South East Asia[3]. This poses a serious challenge to the malaria research community, sparking the need for novel protein targets and molecules against these drug-resistant forms of malaria. FK506, a FDA-approved drug for organ transplant, shows antimalaria efficacy[4,5], but its use is contraindicated owing to its potent immunosuppressive actions. Subsequently, in search for FK506 binding proteins (FKBPs) in the *Plasmodium* species, the piggyback approach led to the identification of the *Plasmodium* FKBP35 in both *P. falciparum* and *P. vivax* (hereafter referred to as *Pf*FKBP35 and *Pv*FKBP35, respectively)[4,6–8].

*Pf*FKBP35 and *Pv*FKBP35 belong to the immunophilin family, more commonly known as FK506 binding proteins (FKBPs). Aside from their immunosuppressive properties, which are mediated via interaction with calcineurin, members of the FKBP family show a canonical peptidyl-prolyl *cis-trans* isomerase (PPIase) or rotamase activity and regulate various physiological functions, including protein folding, stability[9–11], histone chaperone activity[12,13], receptor signaling[14–16], protein trafficking[17,18], transcription[19,20], calcium homeostasis[14,21], spermatogenesis[22], and neuroprotective and neurotrophic activities[23]. These physiological functions emphasize the role of FKBPs as helper proteins in assisting and mediating cell responses to physiological signals and effectors and therefore emerge as potential molecular targets for pharmacological intervention. However, proof of concept study showing the importance of *Plasmodium* FKBP35 for parasite growth is still elusive. Chemical biology approaches have been exploited to verify the role of this protein by employing its high affinity ligand (FK506). Our previous microarray study using FK506 and Cyclosporine as chemical probes has revealed strikingly similar global transcription profiles of *P. falciparum*[24]. This study points out the role of FK506 binding proteins and calcineurin pathway in mediating the parasite growth. Studies from Monaghan *et al.*, have highlighted that the inhibition of either PPIase activity or chaperone activity of FK506 binding proteins without calcineurin inhibition are sufficient to inhibit the growth of *Plasmodium falciparum* 3D7 culture[2]. More importantly, studies from Braun *et al.*, have shown that differences in cellular levels of parasite FKBP35 (100 nM) and the host FKBP12 proteins (5 μM) offer a unique selectivity window to target parasite FKBP proteins in preference to host proteins[5]. Taken together these studies suggest that *Plasmodium* FKBP35 could be a viable drug target for controlling malaria.

Of *Plasmodium* FKBPs, molecular characteristics of *Pf*FKBP35 and *Pv*FKBP35 have been characterized and their catalytic and ligand-binding properties are homologous to other FKBP family members, such as FKBP51 and FKBP52[7,25]. FK506 binding domain of *Plasmodium* FKBPs share sequence and structural similarities with

other canonical FKBP family members (Supplementary Fig. S1). Previously, we have determined the three-dimensional crystal structures of *Pf*FKBD35 and *Pv*FKBD35 in complex with FK506, which offered insights into the molecular interaction between the FK506 and *Plasmodium* FKBD35 proteins[24,26,27]. In our attempts to discover new small molecule inhibitors that could specifically inhibit the parasite PPIase activity, we instigated a structure-based in-silico screening of commercially available library. Based on our *in silico*, crystallographic and NMR studies, coupled with PPIase and malaria growth inhibition assays, here we demonstrate that a purine-like derivative devoid of immunosuppressive activity targets *Plasmodium* FKBP35, inhibits the parasite growth, and possesses potential to be developed as novel therapeutics to combat the malaria.

Results

Identification of N-(2-Ethyl-phenyl)-2-(3H-imidazao [4, 5-b] pyridin-2-yl-sulfanyl)-acetamide as a novel inhibitor of *Plasmodium* FKBPs. *Plasmodium* FKBD35-FK506 crystal complex structures reveal a structural fold, ligand-binding mode similar to those of canonical FKBPs[28,29]. Despite these similarities, the β5-β6 loop (H87, I91) residues in human FKBP12 are varied to Cys106/105 and Ser109/108 residues in *Plasmodium* species. These residues that form the site S2 (Fig. 1c), accommodates the pyranose methyl group of FK506, which is further away from the site S1 (Fig. 1b) while the Trp78 residue (site S1) forms the base for the binding of pipecolyl moiety of FK506. These varied Cys106/105 and Ser109/108 residues are exploited for achieving selectivity towards *Plasmodium* FKBP35. In our structure based pharmacophore modeling, LUDI interaction sites (Fig. 1a) together with excluded volumes (serve to provide the shape or volume of protein active site and to prevent clashes with protein atoms) highlight the explicit hotspots at the active site that are exploited for structure based pharmacophore development. These interaction sites are clustered hierarchically based on the feature type to minimize the number of features that are amenable for pharmacophore development. Two features namely - a hydrophobic anchoring Trp78 and an acceptor at Ile75 of site S1 and similarly three features - an acceptor at Tyr101, a donor at Asp56 and a hydrophobic feature at vicinity of Phe55, Cys106, and Ser109 of site S2, together with exclusion volumes (152) are included in model development. Upon screening our in-house ADME property filtered 3D virtual database of ChemDiv commercial library with this five feature structure based pharmacophore model (Fig. 1d) has enabled a focused library. Together with molecular docking, scoring and consensus results (Supplementary Fig. S2), the library were further prioritized based on their interactions at above mentioned key residues. One of the top ranking ligand N-(2-Ethyl-phenyl)-2-(3H-imidazao [4, 5-b] pyridin-2-ylsulfanyl)-acetamide (referred to as D44), which contains a purine-like ring system linked to a phenyl ring via thio-acetamide linkage (Fig. 2a), selectively inhibits the *Plasmodium* FKBD35 PPIase activity with an IC_{50} of 132 ± 1.09 nM (Fig. 2b) and 125 ± 2.9 nM for *falciparum* and *vivax* species respectively. D44 did not affect the enzymatic

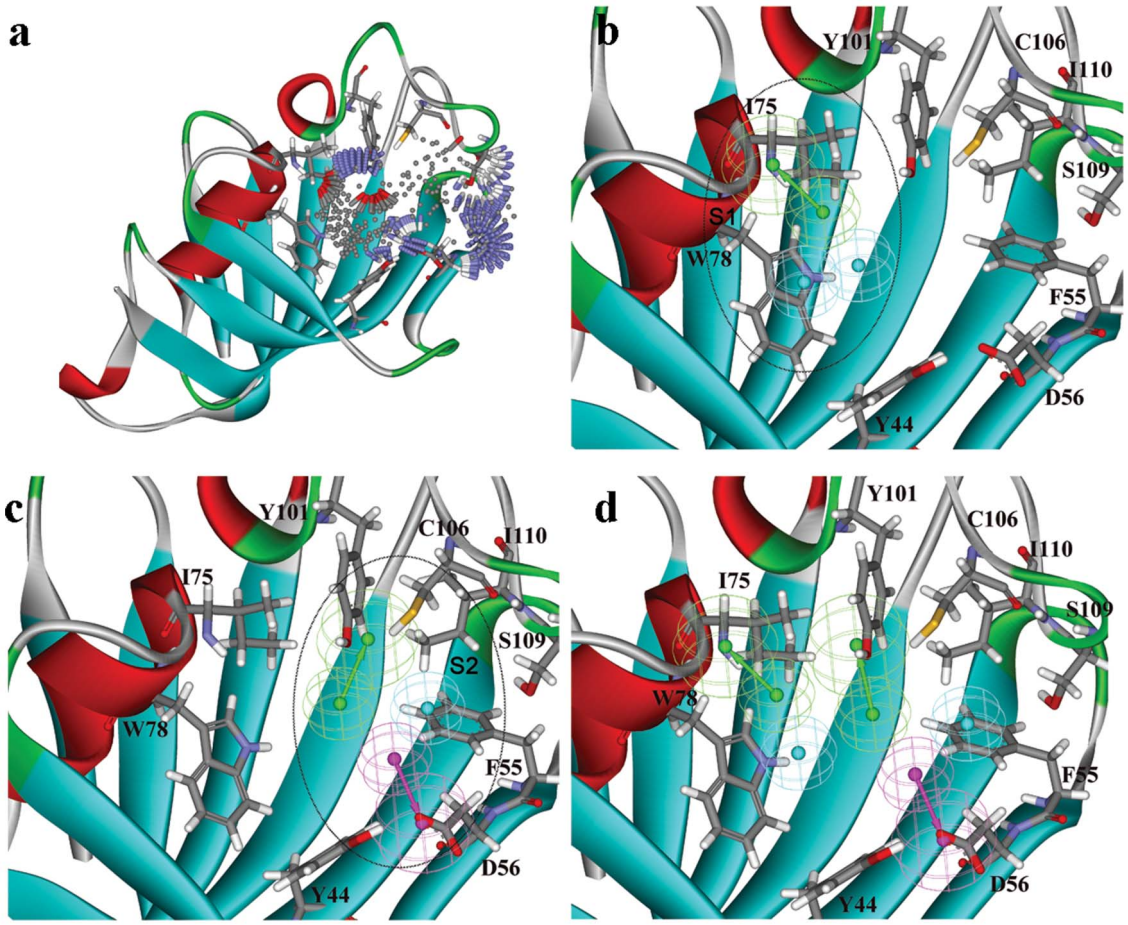

Figure 1 | Structure-based pharmacophore model. (a) Ludi program identifies discrete acceptor (red rods (OH)), donor (purple rods (NH) and hydrophobic (black spheres) vector sites with which a ligand can form efficient interaction with the protein; (b& c) Hierarchical clustering of acceptor, donor, and hydrophobic vector site points enables one to select features targeting select residues as depicted at site S1 (b) and at site S2 (c). (d) Five features were selected targeting specific residues such as F55, D56, I75, W78, and Y101 residues that were included in the structure or receptor based pharmacophore (Exclusion volumes are not shown in figure for clarity).

activity of either human FKBP12 or FKBP52 even at 10 μM concentration (Supplementary Fig. S3). The canonical FKBP ligand FK506 not only inhibits PPIase activity but also inhibits the phosphatase activity of calcineurin[30], by forming a ternary complex with calcineurin, leading to suppression of immune responses. To ascertain that D44 does not interact with calcineurin upon binding to FKBP, calcineurin phosphatase assay is performed and our results demonstrate that D44 weakly binds to human FKBP12 but lacks the ability to interact with calcineurin and inhibit its phosphatase activity (Fig. 2c).

D44 interferes with *P. falciparum* intraerythrocytic growth. To monitor the effects of D44 on *P. falciparum* growth, highly synchronized ring stage (~5 hours post invasion) 3D7 parasites were allowed to grow in the presence of D44 inhibitor at concentration ranging from 1 nM to 1 μM for an entire intraerythrocytic developmental cycle (IDC) from the ring stage through egress and reinvasion, thus providing readout for assessing the inhibitory effects on any part of the erythrocytic cycle. D44 inhibited the growth of *P. falciparum* 3D7 in a dose dependent manner with an IC_{50} of 234.5 ± 1.32 nM. To map the stage specific inhibitory activity of D44, *P. falciparum* 3D7 parasites growth were closely monitored at 8 h time interval for an entire IDC in the presence of D44 and FK506 at ~1 μM and 250 nM respectively (corresponding to ~4× IC_{50}). Parasites morphology at each time point was monitored on Giemsa-stained smears and parasitemia was quantified via flow cytometry. From the ring to early schizont maturation, there is no change in either parasite morphology (Fig. 3a) or parasitemia (Fig. 3b) between the D44- and FK506-treated and control parasites. However during subsequent development, the untreated control parasites successively mature to late schizont and ring stages (Fig. 3a) resulting to an increased parasitemia (Fig. 3b) whereas both D44- and FK506-treated parasites remained arrested at the schizont stage (Fig. 3a) and subsequently degraded leading to a decreased parasitemia, suggesting that D44 interferes with the schizont stage development similar to FK506[24].

To validate this finding, we closely monitored the maturation of early *P. falciparum* 3D7 schizont stage parasites (~36–40 hours post invasion) in presence of D44 or FK506 and in absence of treatment (control). D44 and FK506 treated parasites show significant morphological differences to untreated parasites (Fig. 3c) only after the first 4 hours of schizont maturation. The untreated parasites progresses into their subsequent stages (formation of late schizont and ring stages) while the D44 and FK506 treated parasites remain arrested at the late schizont stage (Fig. 3c) with further degradation of D44-treated parasites (Supplementary Fig. S4). This further corroborates the finding that D44 directly interferes with schizont parasites maturation, probably through a mechanism different from FK506 inhibition.

Furthermore, investigation of the effects of D44 (1 μM) on an additional *P. falciparum* laboratory-adapted strain (Palo Alto) and a field isolate (*Pf*0703) collected from a Senegalese malaria-infected patient and adapted to *in vitro* culture shows that D44 inhibited the growth of both strain in a pattern similar to the 3D7 strain (Fig. 3d). Since the compounds were dissolved in DMSO, we determined the effect of DMSO on parasite growth to discriminate DMSO to compounds specific inhibition and showed no significant DMSO inhibition at 5% dilution (Fig. 3d), suggesting that the observed parasites growth inhibition was D44 specific.

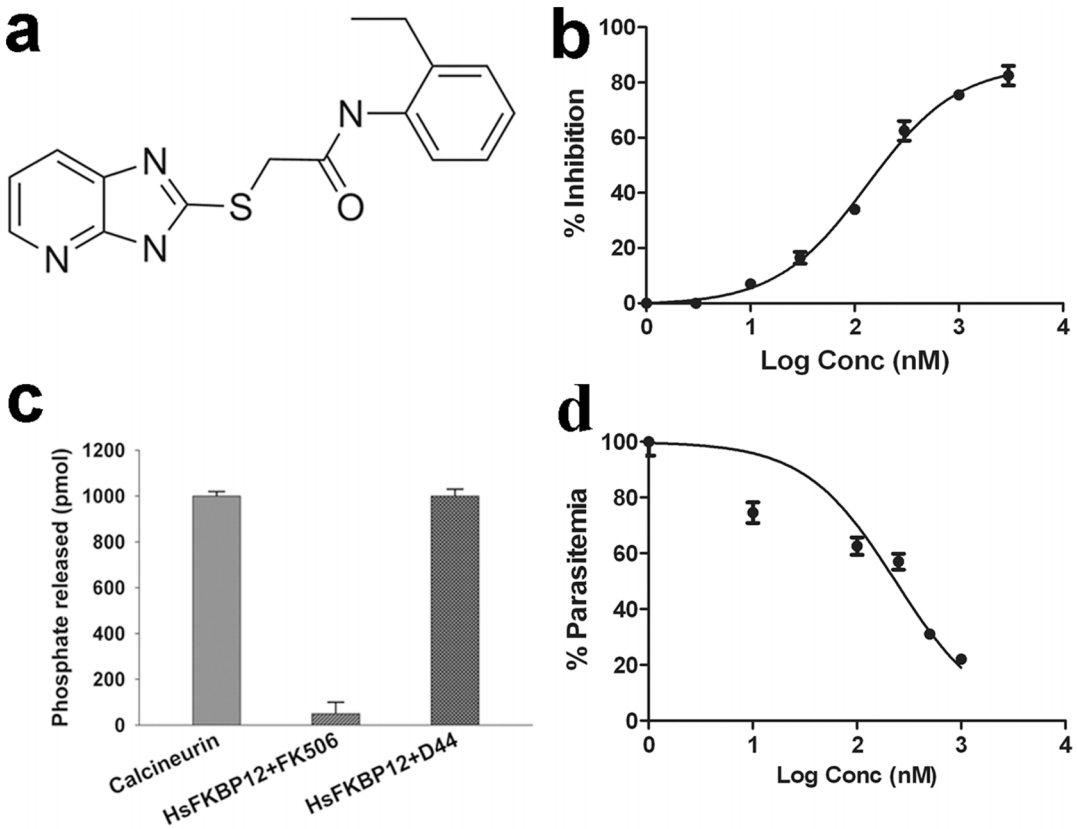

Figure 2 | (a) Chemical structure of ligand D44. (b) Sigmoid dose response curve showing the inhibition of *Pf*FKBD35 enzymatic activity with the increase in concentration of D44. Data is represented as duplicate of two independent experiments ± SEM. (c) Effect of D44 on phosphatase activity of calcineurin. The inhibitory effect of FK506, D44 (5 μM) FKBP12 complexes on the phosphatase activity of calcineurin (CaN) was examined. Calcineurin alone serve as a control. Responses were quantified in terms of phosphate released. (d) Dose dependent inhibition of parasitemia of *Plasmodium falciparum* 3D7 cell line. Error bars represent the SEM of two independent experiments in duplicate.

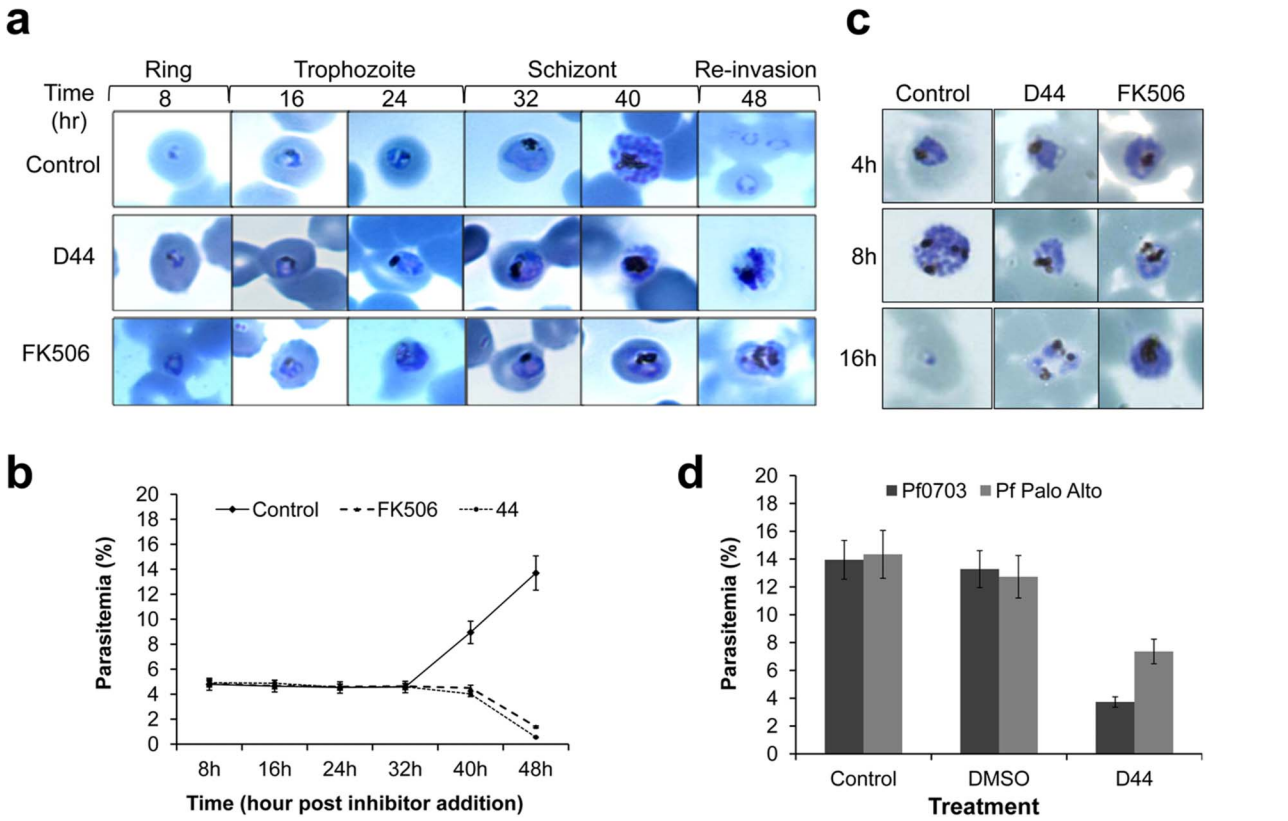

Figure 3 | Effects of D44 treatment on the growth and morphology of different *Plasmodium falciparum* lines (a–b) Morphological characteristics (a) and parasitemia quantification (b) of *P. falciparum* 3D7 parasites growth at 8 h time interval following treatment with either D44 or FK506 showing interference of both inhibitors with the schizont stage development compared to control untreated parasites. Data shown in graph (b) are average of 2 independent experiments performed in triplicate each. (c) Timing and morphological characteristics of the schizont stages inhibition upon incubation with D44 and FK506. During the first 4 h, no significant morphological differences were observed between the treated and control parasites. During the subsequent development, the control parasites progress to the next generation (formation of mature schizont and ring) while the treated cells remain arrested at the late schizont stage. (d) Parasitemia determination of laboratory-strain (*Pf* Palo Alto) and field isolate (*Pf*0703) after a complete IDC (48 hrs) in presence of D44 or controls DMSO-treated and untreated parasites. D44 significantly inhibits growth of both parasites strains similar to 3D7 line.

Crystallographic structures of *Plasmodium* FKBD35 in complex with D44. To gain better structural insights into the mode of action of D44, X-ray crystallographic structures of *Pf*FKBD35 and *Pv*FKBD35 in complex with D44 were determined to a resolution of 2.75 Å and 1.73 Å, respectively. Refined crystallographic structure revealed a topology consisting of six β-stranded sheets and a short α-helix similar to the previous *Plasmodium* FKBD35-FK506 structures from *P. falciparum* (PDB ID 2VN1)[24] and *P. vivax* (PDB ID 3IHZ)[26]. The *Pf*FKBD35-D44 complex consists of three monomers in the asymmetric unit (Fig. 4a) with chains A and B forming a covalent dimer via an intermolecular disulphide bond between Cys106 from both the chains. Similarly the third monomer (chain C) also forms an identical dimer with the neighboring chain, which is generated by crystal packing. While *Pv*FKBD35-D44 complex consisted of one monomer in the asymmetric unit (Fig. 4b) forming a dimer with the neighboring chain, generated by crystal packing, with the help of a disulphide bond through Cys105. The *Pf* and *Pv*FKBD35 structures superpose well with a backbone root-mean-square deviation (RMSD) of 0.314 Å.

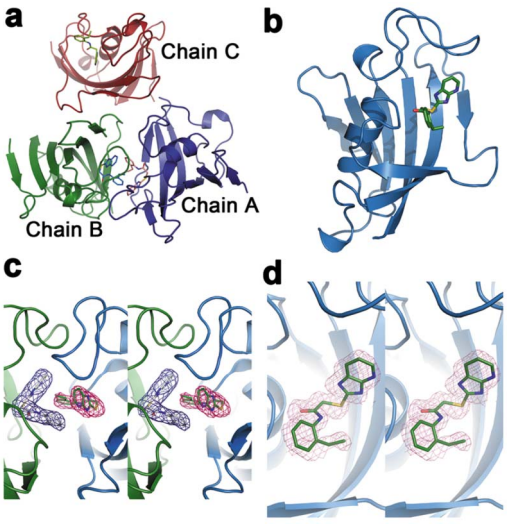

Figure 4 | **The crystal structures of *Plasmodium* FKBD35 in complex with the ligand D44.** The cartoon representation of the asymmetric units of *Pf*FKBD35 (a) and *Pv*FKBD35 (b) in complex with ligand D44 (in stick mode), showing the three chains and a single chain respectively. 2Fo-Fc difference Fourier map contoured at 1 σ cut-off of ligand D44 in complex with *Pf*FKBD35 (c) and *Pv*FKBD35 (d), in stereo mode. Figures were generated using the program *PyMOL*[65].

Discussion

Our ligand design was mainly aimed to target the two highly conserved Cys106/105 and Ser109/108 residues within the *P. falciparum and P. vivax* species to achieve selectivity towards *Plasmodium* FKBP35 (Supplementary Fig. S1). Virtual screening with structure or receptor based pharmacophore model with exclusion volumes are

shown to map hits that are complementary to the active site and improve the hit rate by filtering the false positives[31]. Ligands which are predicted to have interaction at both sites S1 and S2 and in consensus with most of the scoring functions are selected for experimental screening. Inhibition of substrate activity of the PPIase provides a convenient assay to evaluate whether the ligands bind and inhibit the enzymatic activity of the protein. D44 potently inhibits the PPIase activity of *P. falciparum/vivax* FKBP35 at sub-micromolar concentration (132 nM/125 nM) selectively and show ~100 fold selectivity towards parasite FKBPs over human FKBPs. D44 not only inhibits the *in vitro* growth of *Plasmodium falciparum* 3D7 strain parasite at 234.5 ± 1.32 nM (Fig. 2d) but also the growth of Palo Alto strain and field isolate of *Pf*0703 (Essai 15/05/2013, collected from a Senegalese malaria infected patient) by 50% at 1 μM concentration. These data suggests that D44 can inhibit the PPIase activity of FKBP35 at sub-micromolar range and hinder the growth of different strains of *Plasmodium falciparum* at micromolar range. Further lead optimization studies are needed to improve the efficacy of its anti-malaria properties. D44 exhibited low cytotoxicity on HeLa and HTC116 cancer cell lines and their cell proliferation was inhibited albeit at much higher concentrations with an IC_{50} of 465 ± 3.16 μM and 343.6 ± 1.26 μM respectively, suggesting 1000 fold selectivity towards malaria parasite (Supplementary Fig. S5). It is important to note that direct evidence linking the inhibition of PPIase activity to growth of parasite is lacking, nonetheless many studies on human orthologues have shown the importance of FKBPs in regulation of cell cycle[16], transcription[19,20] and histone methylation[12,13]. Further studies using chemical biology approaches using selective *Plasmodium* FKBP ligands like D44 are awaited to delineate the role of FKBPs or its substrate protein interactions that might be critical to the growth and survival of the malaria parasite.

Comparison to previously determined apo form NMR structures[6,26] indicate a well conserved structural fold with an RMSD of 2.28 Å and 1.37 Å for *Pf*FKBD35 and *Pv*FKBD35, respectively (Supplementary Fig. S6a–b). As anticipated, the ligand flanking loops namely β3-β4, β4-α1, and β5-β6 undergo small structural changes leading to an increase in accessible surface area (Supplementary Fig. S6a–b). The psi angle of Phe55 undergoes a change from 124° (apo form) to −21° (D44) which is 6°/2.6° more than the FK506 complex in *Plasmodium falciparum/vivax* structures respectively. These changes could well be attributed to the non-bonded contacts made by D44 with Phe55/54, unlike the hydrogen-bonded contacts of FK506, which gives the residues more flexibility. The electron density for D44 (Fig. 4c, d) was traced unequivocally in the electron density difference map in the hydrophobic binding site. One ligand per monomer was observed, sitting in the dimer interface facing each other separated by a distance of 3.6–4.2 Å. Crystallographic structures of *Pf*FKBD35 and *Pv*FKBD35 in complex with D44 showed that the purine like ring of D44 makes critical hydrogen bonding contacts with the catalytic residues Asp56/55 and Tyr101/100 (Fig. 5a, b) and the thio-acetamide linker of D44 through its carbonyl group interacts with Ile75/74, locking the ligand in the active site pocket (Fig. 5a, b & c) (Table S1). Further non-bonded contacts (Fig. 5a, b) with residues like Phe55/54, Phe65/64, Trp78/77, and Ile110/109 stabilize the ligand-bound complexes (Table S1).

Our 2D $^{1}H,^{15}N$ heteronuclear single quantum correlation (HSQC) nuclear magnetic spectroscopy (NMR) results confirmed that most of the active site residues including the Phe65, Trp78 residues show chemical shift perturbation upon binding with D44 (Supplementary Fig. S7). Superimposition FKBD35-D44 structures to apo form structures[6,26] not only reveal a translation of ~2–6.8 Å (Fig. 5d) on

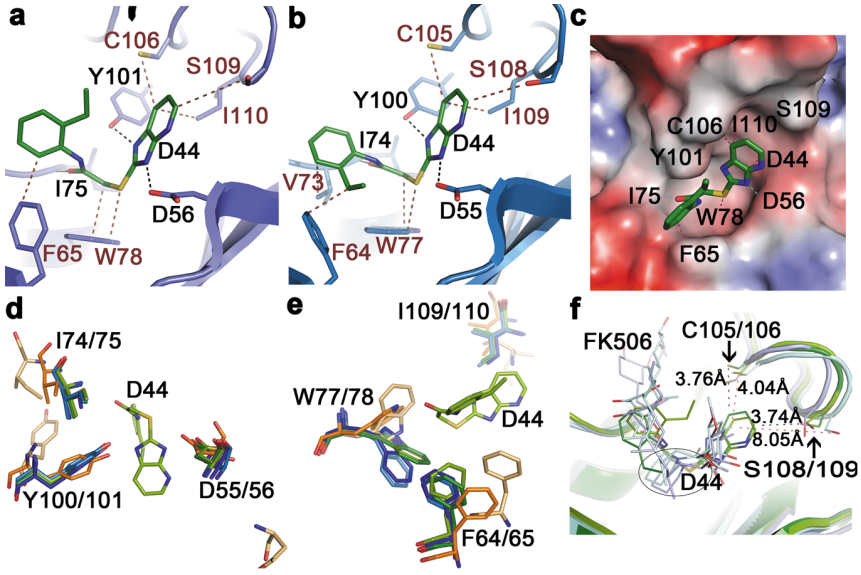

Figure 5 | Comparison of binding site interactions. (a & b) The stick representation of residues making hydrogen bonds (black) and the non-bonded contacts (brown) with ligand D44 in *Pf*FKBD35 (a) and *Pv*FKBD35 (b). Ser 109/108, one of the highly conserved residues is also shown for clarity; (c) Electrostatic surface representation of *Pf*FKBD35 in complex with D44 (in stick mode), showing the docking of the ligand into the hydrophobic active site cleft; (d & e) Superposition of interacting residues of apo (*Pf* - light orange; *Pv* - orange) FKBD35 with their corresponding FK506 (*Pf* – light green; *Pv* – green) and D44 (*Pf* – light blue; *Pv* – dark blue) complexes. The D44 of *Pf*FKBD35 alone is also shown for clarity. Large deviations in hydrogen bonded residues can be observed for *Pf*FKBD35 compared to its *P.vivax* counterpart (d). While the residues involved in non-bonded contacts (e) clearly show a movement away from the active site as the ligand gets bigger, compared to the apo form; (f) Specificity of ligand D44 towards the highly conserved Cys 106/105 and Ser 109/108 can be observed when superposed with the corresponding FK506 structures. D44 (*Pf* – light green; *Pv* – dark green) clearly moves closer to Cys 109/108 compared to FK506 (*Pf* – light blue; *Pv* – cyan). The distances are shown for the *Pv*FKBD35, with D44 at 3.76 and 3.74 Å from Cys 105 and Ser 108 respectively, compared to 4.04 and 8.05 Å in FK506. In addition, the hydroxyl group of Ser108 flips towards the ligand (b & e) in *Pv*FKBD35 structure enhancing the ligand specificity. It could also be noticed that the thio-acetamide linker in D44 compensates for the pipecolinyl moiety (shown within the black open circle) of FK506, a unique feature pertaining to D44. In figure 5 d, e & f the residues are labeled according to their species, namely *Pf/Pv*. The figures were generated using the program *PyMOL*[65].

residues involved in hydrogen bonded interactions, but also noticeable changes in the local conformations of Phe65/64 and Trp78/77 side chains (Fig. 5e). Quantitative comparison of ligand bound structures of *Plasmodium* FKBDs indicate that the Phe65/64 moves by ~4/2.8 Å and ~5.5/3.5 Å in complex with D44 and FK506, respectively, while Trp78/77 sways by ~6/5.7 Å and ~7.5/5.9 Å (Fig. 5e). In addition, directionality can be conferred as these two residues approximate towards the thio-acetamide due to the strong hydrophobic interactions of sulphur with the hydrophobic residues (Fig. 5e). In *Pf*FKBD35, D44 is much closer (Fig. 5f) to the nearest atom from the purine like ring located at a distance of 3.6 Å and 4.3 Å from Cys106 and Ser109 respectively, compared to 3.9 Å and 5.4 Å in the corresponding FK506 complex. Similarly in *Pv*FKBD35, Cys105 and Ser108 are at a distance of 3.76 Å and 3.74 Å from D44, compared to 4.04 and 8.05 Å in its FK506 (Fig. 5f) complex. The hydroxyl group of Ser108 in *Pv*FKBD35 flips towards purine like ring of D44 (Fig. 5b, f) due to close van der Waal contacts with this residue which is well conserved among the *Plasmodium* species, thereby enhancing its selectivity towards *Plasmodium* FKBPs. Structure activity relationship studies on FKBP12 inhibitors[32,33] have shown the presence of pipecolinyl or proline moiety being paramount for the binding and inhibition of enzymatic activity. Here, we present a unique chemotype which possesses a thio-acetamide compensating the lack of bulky pipecolinyl group (Fig. 5f) and through its hydrophobic interactions induce local conformational changes (Fig. 5e, f) at the active site. Overall, though D44 (MW of 312) is smaller in size compared to FK506 (MW of 804), it interacts with specific residues as predicted, confirming that these interactions between the protein and ligand are critical for the inhibition of the enzyme.

Taken together, we have identified a novel small molecule *Plasmodium* FKBP35 antagonist and demonstrated its biological activity in *P. falciparum*. The elucidation of crystal structures of *Plasmodium* FKBD35 in complex with D44 further substantiates the efficiency of ligand to target not only *P. falciparum* but also *P. vivax*, a much neglected target whose incidence is re-emerging with drug resistant forms and gaining awareness[34,35]. Thus, the information presented in the current study could be used to aid designing selective small molecule inhibitors that bind to the parasite FKBP and potentially antagonize their function in the parasite life cycle.

Methods

Structure-based pharmacophore. *Pf*FKBD35-FK506 X-ray crystal structure (PDB ID 2VN1) was prepared by correcting bond orders, missing atoms and energy minimized using conjugate gradient force field. Ludi interaction map[36–38] was generated around 10 Å of the active site residues using three features - acceptor, donor and lipophilic features highlighting the probable interaction sites for the ligands with the protein atoms. Features anchoring residues like Asp56, Trp78, Tyr101, and Cys106 are included in structure based pharmacophore model. To avoid clashes of ligand with the protein atoms, a total of 152 exclusion volumes are incorporated into the structure based pharmacophore model[37]. Pharmacophore screening on ChemDiv library resulted in a focused library of 13,000 molecules. This library is further processed by applying ADME filters which refined the library to ~2600 molecules.

Virtual screening and consensus scoring. An advanced molecular docking program GOLD v4.0[39] was employed in docking the focused library into the active site of *Pf*FKBP35. Docking parameters were optimized to simulate the crystal ligand conformation and the same parameters were used for screening the focused library. Thus obtained docking solutions were not only scored with default gold scoring function, but also rescored with Ligscore[38], PLP[40], JAIN[41], LUDI[36], and PMF[42,43] scoring functions in Accelrys suite. A consensus scoring scheme[44–49] was applied to remove any bias or inadequacies of using one particular scoring function. Upon visual inspection of 500 top scoring molecules, compounds were prioritized for contact to key catalytic residues like Asp56, Tyr101, and Ile75 and accordingly 46 compounds were purchased and tested experimentally (Supplementary Fig. S2).

PPIase assay. PPIase activity was assessed in the presence and absence of inhibitors by the method described earlier[50] using Succ-Ala-Leu-Pro-Phe-p-nitroaniline as a substrate (Peptide Institute, Osaka, Japan). All the reagents were pre-equilibrated at 0°C. The final reaction mixture (1 mL) contained 100 nM of *Pf*FKBD35 or human FKBP12/FKBP52 (100 nM), 100 μM of substrate and 300 μg of α-chymotrypsin (Sigma, St. Louis, MO) and assay buffer (50 mM HEPES, 100 mM NaCl, pH 8.0 at 0°C). Reaction was performed at 4°C and the changes in the absorbance were monitored at 390 nm for 3 min on a Shimadzu UV-1800 UV-vis spectrophotometer. IC_{50} was calculated from dose response curve in duplicate using GraphPad Software[51].

Calcineurin assay. Calcineurin assay was carried out using recombinant human calcineurin as described previously[52–56], with some modifications. Reactions (50 μl) contained 50 mM Tris-HCl (pH 7.5), 100 mM NaCl, 6 mM $MgCl_2$, 0.5 mM $CaCl_2$, 0.1 mg/ml BSA, 0.5 mM DTT, 0.025% NP-40, 0.25 μM calmodulin, *Hs*FKBP12, 5 μM FK506 and D44, 0.5 μM RII phosphopeptide (a specific calcineurin substrate). Reaction mixtures were incubated for 10–30 min at 30°C before the addition of the substrate peptide to initiate dephosphorylation at 30°C. The reaction was terminated by addition of Malachite Green. The reaction was monitored by reading the absorbance at 620 nm.

Growth inhibition assays. *P. falciparum* laboratory strains (3D7 and Palo Alto) and field isolate (*Pf*0703) were used in this study to investigate the effects of D44 on parasites growth. The *Pf*0703field isolate was isolated from a Senegalese malaria-infected patient and adapted to *in vitro* in the laboratory at the Pasteur Institute of Dakar. Parasites (5% parasitemia, 2% hematocrit) at the mid ring stage (~6–10 hours post-invasion, hpi) were incubated in triplicate in a 96 well plate with 250 nM of FK506 or 1 μM of D44 or in absence of treatment (control). Parasites maturation was monitored every 8 h for an entire Intraerythrocytic Developmental Cycle (IDC) by Giemsa staining of fixed smears for comparison of parasite morphology at each time point. Parasitemia was quantified by flow cytometry based assay using either Ethidium Bromide (1/1000) (for 3D7) or Sybr Green I (1/1000) (for Palo Alto and *Pf*0703) DNA stain dyes. Briefly, parasites were incubated with selected either dye in PBS for 1hour at room temperature, washed 3 times with PBS then resuspended in PBS. Wells content were separately transferred to a FACS tube and parasitemia was quantified through a FACS Calibur with an acquisition of 10.000 events/sample.

Monitoring of stage specific effects of D44 and FK506 was carried out by incubating separately highly synchronized ring, trophozoite or schizont stages of *P. falciparum* 3D7 parasites with FK506 (250 μM), D4 (1 μM) or without inhibitor (control) for 24 h, duration sufficient to allow transition to the next stage. After 8 h of incubation, drugs were removed, parasites were washed twice with PBS, then fresh growth medium was added into the culture and parasites were allowed to mature for an additional 16 h. Parasite morphology and parasitemia were determined as described above.

Cell proliferation assay. HeLa, HTC116 cell lines were maintained in Dulbecco's Modified Eagle Medium (DMEM) containing 10% fetal bovine serum, 1% penicillin/streptomycin and maintained at 37°C in a humidified 5% CO_2 chamber. Cell proliferation was determined using the CellTiter 96® AQueous One Solution Cell Proliferation Assay kit (Promega, Madison, WI, USA). This assay uses a colorimetric method to determine the number of viable cells. Briefly, 5×10^3 cells/well were seeded in a 96-well plate. The volume of the media in each well was 100 μl. Cells were maintained in a humidified, 5% CO_2 atmosphere till the monolayers reached 50–60% confluency (24–36 h). Cells were then incubated with D44 for another 72 h. At the end of this period, 20 μl/well of the reagent was added to the cells, incubated for another 1–4 h and absorbance was measured at 490 nm in a 96-well plate reader. The values shown are the mean ± SEM of at least three independent experiments performed in triplicates. IC50 were calculated based on A490 (as % control of untreated cells).

Crystallization, X-ray data collection, structure determination and refinement. *Pf*FKBD35 and *Pv*FKBD35 were expressed and purified as described previously[26] and was used for crystallization at a concentration of 15 mg/ml. Initially, a series of ligands were screened for crystallization as a cocktail containing two or three ligands; the cocktail approach proved screening for initial crystal hits efficient and comprehensive[57]. The cocktail of ligands were incubated overnight with the protein at a molar ratio of 1 : 1. This protein-cocktail complex was screened using an ammonium sulphate-buffer grid. After 2 weeks, rod shaped crystals appeared in 3.5 M ammonium sulphate and 0.1 M citrate buffer, pH 5.5 with *Pf*FKBD35-D44 containing cocktail. Further optimization with D44 alone yielded bigger crystals in 3.5 M ammonium sulphate and 0.1 M citrate buffer, pH 5.75. Similarly, the *Pv*FKBD35-D44 crystals grew in 3.0 M ammonium sulphate and 0.1 M bicine, pH 9.0. Both crystals were cryo-protected with 20% glycerol added to their corresponding mother liquors and flash-frozen at 100 K during data collection. Data for *Pf*FKBD35-D44 from a single crystal up to 2.75 Å were collected at 100 K on beamline 13B1 at the National Synchrotron Radiation Research Center (Hsinchu, Taiwan) using ADSC-Quantum 315 detector at a wavelength of 0.9642Å. While data up to 1.73 Å was collected from a single crystal of *Pv*FKBD35-D44 using Rigaku R-Axis IV image plate mounted on a Rigaku Micromax-007 HF X-ray generator with CuK^{α} radiation. The diffraction data was indexed, integrated and scaled using the HKL2000[58] suite of programs and d*TREK[59]. The *Pf*FKBD35-D44 crystal belonged to the tetragonal space group $P4_32_12$, similar to the previously solved *Pf*FKBD35-FK506 complex[24] (PDB ID 2VN1). The Mathews co-efficient indicated the presence of three monomers in the asymmetric unit, due to an enlarged unit cell. Therefore, a molecular replacement search was employed using the program PHASER[60], with a monomer unit of the *Pf*FKBD35-FK506 (PDB ID 2VN1). PHASER identified the three monomers in the asymmetric unit. A similar protocol was adapted for *Pv*FKBD35-D44 data which belonged to the trigonal space group $P3_221$, with one molecule in the asymmetric unit located using the program PHASER with a monomer unit of *Pv*FKBD35-FK506 (PDB ID 3IHZ)[26] as the search model. In both structures, after

initial refinement using REFMAC[61], the electron density was observed for D44 in the Fo-Fc difference Fourier map at 3 σ cut-off. Further cycles of map fitting using the program COOT[62], followed by refinement, resulted in the final structure with good geometry and stereochemistry. A few missing residues were observed at the terminal ends of the protein. The program MOLPROBITY[63] showed none of the residues outside the Ramachandran plot[64]. The data collection and refinement statistics are given in Table S2. All structural data, including structure factors where applicable, have been deposited into the Protein Data Bank with PDB codes 4J4N & 4J4O.

Chemical shift perturbation analysis by NMR spectroscopy. To study the ligand-protein interactions, chemical shift perturbations to ^{15}N- labeled *Plasmodium* FKBD35 were monitored on 2D HSQC spectra recorded at 298K on a Bruker Avance 700. For this, 0.1 mM protein samples in 20 mM sodium phosphate, pH6.5 were used and chemical shift perturbations were analyzed by adding an excess amount of the ligand D44.

1. Gardner, M. J. *et al.* Genome sequence of the human malaria parasite Plasmodium falciparum. *Nature* **419**, 498–511 (2002).
2. Monaghan, P., Fardis, M., Revill, W. P. & Bell, A. Antimalarial effects of macrolactones related to FK520 (ascomycin) are independent of the immunosuppressive properties of the compounds. *J Infect Dis* **191**, 1342–9 (2005).
3. Dondorp, A. M. *et al.* The Threat of Artemisinin-Resistant Malaria. *New England Journal of Medicine* **365**, 1073–1075 (2011).
4. Bell, A., Wernli, B. & Franklin, R. M. Roles of peptidyl-prolyl cis-trans isomerase and calcineurin in the mechanisms of antimalarial action of cyclosporin A, FK506, and rapamycin. *Biochem Pharmacol* **48**, 495–503 (1994).
5. Braun, P. D. *et al.* A bifunctional molecule that displays context-dependent cellular activity. *J Am Chem Soc* **125**, 7575–80 (2003).
6. Kang, C. B., Ye, H., Yoon, H. R. & Yoon, H. S. Solution structure of FK506 binding domain (FKBD) of Plasmodium falciparum FK506 binding protein 35 (PfFKBP35). *Proteins* **70**, 300–2 (2008).
7. Kumar, R., Adams, B., Musiyenko, A., Shulyayeva, O. & Barik, S. The FK506-binding protein of the malaria parasite, Plasmodium falciparum, is a FK506-sensitive chaperone with FK506-independent calcineurin-inhibitory activity. *Mol Biochem Parasitol* **141**, 163–73 (2005).
8. Monaghan, P. & Bell, A. A Plasmodium falciparum FK506-binding protein (FKBP) with peptidyl-prolyl cis-trans isomerase and chaperone activities. *Mol Biochem Parasitol* **139**, 185–95 (2005).
9. Barth, S. *et al.* The peptidyl prolyl cis/trans isomerase FKBP38 determines hypoxia-inducible transcription factor prolyl-4-hydroxylase PHD2 protein stability. *Mol Cell Biol* **27**, 3758–68 (2007).
10. Choi, B. H., Feng, L. & Yoon, H. S. FKBP38 protects Bcl-2 from caspase-dependent degradation. *J Biol Chem* **285**, 9770–9 (2010).
11. Jinwal, U. K. *et al.* The Hsp90 cochaperone, FKBP51, increases Tau stability and polymerizes microtubules. *J Neurosci* **30**, 591–9 (2010).
12. Kuzuhara, T. & Horikoshi, M. A nuclear FK506-binding protein is a histone chaperone regulating rDNA silencing. *Nat Struct Mol Biol* **11**, 275–83 (2004).
13. Nelson, C. J., Santos-Rosa, H. & Kouzarides, T. Proline isomerization of histone H3 regulates lysine methylation and gene expression. *Cell* **126**, 905–16 (2006).
14. Cameron, A. M. *et al.* Immunophilin FK506 binding protein associated with inositol 1,4,5-trisphosphate receptor modulates calcium flux. *Proc Natl Acad Sci U S A* **92**, 1784–8 (1995).
15. Riggs, D. L. *et al.* The Hsp90-binding peptidylprolyl isomerase FKBP52 potentiates glucocorticoid signaling in vivo. *EMBO J* **22**, 1158–67 (2003).
16. Wang, T. *et al.* The immunophilin FKBP12 functions as a common inhibitor of the TGF beta family type I receptors. *Cell* **86**, 435–44 (1996).
17. Ahearn, I. M. *et al.* FKBP12 binds to acylated H-ras and promotes depalmitoylation. *Mol Cell* **41**, 173–85 (2011).
18. Shirane, M. & Nakayama, K. I. Inherent calcineurin inhibitor FKBP38 targets Bcl-2 to mitochondria and inhibits apoptosis. *Nat Cell Biol* **5**, 28–37 (2003).
19. Ochocka, A. M. *et al.* FKBP25, a novel regulator of the p53 pathway, induces the degradation of MDM2 and activation of p53. *FEBS Lett* **583**, 621–6 (2009).
20. Yang, W. M., Inouye, C. J. & Seto, E. Cyclophilin A and FKBP12 interact with YY1 and alter its transcriptional activity. *J Biol Chem* **270**, 15187–93 (1995).
21. Jayaraman, T. *et al.* FK506 binding protein associated with the calcium release channel (ryanodine receptor). *J Biol Chem* **267**, 9474–7 (1992).
22. Crackower, M. A. *et al.* Essential role of Fkbp6 in male fertility and homologous chromosome pairing in meiosis. *Science* **300**, 1291–5 (2003).
23. Edlich, F. *et al.* The specific FKBP38 inhibitor N-(N',N'-dimethylcarboxamidomethyl)cycloheximide has potent neuroprotective and neurotrophic properties in brain ischemia. *J Biol Chem* **281**, 14961–70 (2006).
24. Kotaka, M. *et al.* Crystal structure of the FK506 binding domain of Plasmodium falciparum FKBP35 in complex with FK506. *Biochemistry* **47**, 5951–61 (2008).
25. Galat, A. Peptidylprolyl cis/trans isomerases (immunophilins): biological diversity--targets--functions. *Curr Top Med Chem* **3**, 1315–47 (2003).
26. Alag, R. *et al.* NMR and crystallographic structures of the FK506 binding domain of human malarial parasite Plasmodium vivax FKBP35. *Protein Sci* **19**, 1577–86 (2010).
27. Alag, R., Shin, J. & Yoon, H. S. NMR assignments of the FK506-binding domain of FK506-binding protein 35 from Plasmodium vivax. *Biomol NMR Assign* **3**, 243–5 (2009).
28. Van Duyne, G. D., Standaert, R. F., Karplus, P. A., Schreiber, S. L. & Clardy, J. Atomic structure of FKBP-FK506, an immunophilin-immunosuppressant complex. *Science* **252**, 839–42 (1991).
29. Van Duyne, G. D., Standaert, R. F., Karplus, P. A., Schreiber, S. L. & Clardy, J. Atomic structures of the human immunophilin FKBP-12 complexes with FK506 and rapamycin. *J Mol Biol* **229**, 105–24 (1993).
30. Mukai, H. *et al.* FKBP12-FK506 complex inhibits phosphatase activity of two mammalian isoforms of calcineurin irrespective of their substrates or activation mechanisms. *J Biochem* **113**, 292–8 (1993).
31. Greenidge, P. A., Carlsson, B., Bladh, L. G. & Gillner, M. Pharmacophores incorporating numerous excluded volumes defined by X-ray crystallographic structure in three-dimensional database searching: application to the thyroid hormone receptor. *J Med Chem* **41**, 2503–12 (1998).
32. Hamilton, G. S. & Steiner, J. P. Immunophilins: beyond immunosuppression. *J Med Chem* **41**, 5119–43 (1998).
33. Wang, X. J. & Etzkorn, F. A. Peptidyl-prolyl isomerase inhibitors. *Biopolymers* **84**, 125–46 (2006).
34. Bassat, Q. & Alonso, P. L. Defying malaria: Fathoming severe Plasmodium vivax disease. *Nat Med* **17**, 48–9 (2011).
35. Carlton, J. M., Sina, B. J. & Adams, J. H. Why is Plasmodium vivax a neglected tropical disease? *PLoS Negl Trop Dis* **5**, e1160 (2011).
36. Bohm, H. J. LUDI: rule-based automatic design of new substituents for enzyme inhibitor leads. *J Comput Aided Mol Des* **6**, 593–606 (1992).
37. Kirchhoff, P. D., Brown, R., Kahn, S., Waldman, M. & Venkatachalam, C. M. Application of structure-based focusing to the estrogen receptor. *Journal of Computational Chemistry* **22**, 993–1003 (2001).
38. Venkatachalam, C. M., Jiang, X., Oldfield, T. & Waldman, M. LigandFit: a novel method for the shape-directed rapid docking of ligands to protein active sites. *J Mol Graph Model* **21**, 289–307 (2003).
39. Jones, G., Willett, P., Glen, R. C., Leach, A. R. & Taylor, R. Development and validation of a genetic algorithm for flexible docking. *J Mol Biol* **267**, 727–48 (1997).
40. Gehlhaar, D. K. *et al.* Molecular recognition of the inhibitor AG-1343 by HIV-1 protease: conformationally flexible docking by evolutionary programming. *Chem Biol* **2**, 317–24 (1995).
41. Jain, A. N. Scoring noncovalent protein-ligand interactions: a continuous differentiable function tuned to compute binding affinities. *J Comput Aided Mol Des* **10**, 427–40 (1996).
42. Muegge, I. PMF scoring revisited. *J Med Chem* **49**, 5895–902 (2006).
43. Muegge, I. & Martin, Y. C. A general and fast scoring function for protein-ligand interactions: a simplified potential approach. *J Med Chem* **42**, 791–804 (1999).
44. Carta, G., Knox, A. J. & Lloyd, D. G. Unbiasing scoring functions: a new normalization and rescoring strategy. *J Chem Inf Model* **47**, 1564–71 (2007).
45. Cheng, T., Li, X., Li, Y., Liu, Z. & Wang, R. Comparative assessment of scoring functions on a diverse test set. *J Chem Inf Model* **49**, 1079–93 (2009).
46. Clark, R. D., Strizhev, A., Leonard, J. M., Blake, J. F. & Matthew, J. B. Consensus scoring for ligand/protein interactions. *J Mol Graph Model* **20**, 281–95 (2002).
47. Oda, A., Tsuchida, K., Takakura, T., Yamaotsu, N. & Hirono, S. Comparison of consensus scoring strategies for evaluating computational models of protein-ligand complexes. *J Chem Inf Model* **46**, 380–91 (2006).
48. Teramoto, R. & Fukunishi, H. Supervised consensus scoring for docking and virtual screening. *J Chem Inf Model* **47**, 526–34 (2007).
49. Wang, R., Lu, Y. & Wang, S. Comparative evaluation of 11 scoring functions for molecular docking. *J Med Chem* **46**, 2287–303 (2003).
50. Fischer, G., Bang, H. & Mech, C. Determination of enzymatic catalysis for the cis-trans-isomerization of peptide binding in proline-containing peptides. *Biomed Biochim Acta* **43**, 1101–11 (1984).
51. Harvey, M. & Christopoulos, A. *Fitting Models to Biological Data using Linear and Nonlinear Regression. A Practical Guide to Curve Fitting* (Oxford University Press, New York, New York, 2004).
52. Donella-Deana, A., Krinks, M. H., Ruzzene, M., Klee, C. & Pinna, L. A. Dephosphorylation of phosphopeptides by calcineurin (protein phosphatase 2B). *Eur J Biochem* **219**, 109–17 (1994).
53. Enz, A., Shapiro, G., Chappuis, A. & Dattler, A. Nonradioactive assay for protein phosphatase 2B (calcineurin) activity using a partial sequence of the subunit of cAMP-dependent protein kinase as substrate. *Anal Biochem* **216**, 147–53 (1994).
54. Harder, K. W. *et al.* Characterization and kinetic analysis of the intracellular domain of human protein tyrosine phosphatase beta (HPTP beta) using synthetic phosphopeptides. *Biochem J* **298**(Pt 2), 395–401 (1994).
55. Martin, B., Pallen, C. J., Wang, J. H. & Graves, D. J. Use of fluorinated tyrosine phosphates to probe the substrate specificity of the low molecular weight phosphatase activity of calcineurin. *J Biol Chem* **260**, 14932–7 (1985).
56. Mondragon, A. *et al.* Overexpression and purification of human calcineurin alpha from Escherichia coli and assessment of catalytic functions of residues surrounding the binuclear metal center. *Biochemistry* **36**, 4934–42 (1997).
57. Bosch, J. *et al.* Using fragment cocktail crystallography to assist inhibitor design of Trypanosoma brucei nucleoside 2-deoxyribosyltransferase. *J Med Chem* **49**, 5939–46 (2006).

58. Otwinowski, Z. & Minor, W. Processing of X-ray Diffraction Data Collected in Oscillation Mode. *Methods in Enzymology* **276**, 307–326 (1997).
59. Pflugrath, J. W. The finer things in X-ray diffraction data collection. *Acta Crystallogr D Biol Crystallogr* **55**, 1718–25 (1999).
60. McCoy, A. J. *et al*. Phaser crystallographic software. *J Appl Crystallogr* **40**, 658–674 (2007).
61. Murshudov, G. N. *et al*. REFMAC5 for the refinement of macromolecular crystal structures. *Acta Crystallogr D Biol Crystallogr* **67**, 355–67 (2011).
62. Emsley, P. & Cowtan, K. Coot: model-building tools for molecular graphics. *Acta Crystallogr D Biol Crystallogr* **60**, 2126–32 (2004).
63. Chen, V. B. *et al*. MolProbity: all-atom structure validation for macromolecular crystallography. *Acta Crystallogr D Biol Crystallogr* **66**, 12–21 (2010).
64. Ramachandran, G. N., Ramakrishnan, C. & Sasisekharan, V. Stereochemistry of polypeptide chain configurations. *J Mol Biol* **7**, 95–9 (1963).
65. DeLano, W. L. The PyMOL Molecular Graphics System. *DeLano Scientific, Palo Alto, CA, USA* (2002).

Acknowledgements

We thank Dr. Shin Joon for his assistance in NMR data collection and helpful discussions during analysis of NMR data. We also thank Dr. Malathy Sony and Professor Gerhard Gruber for collecting the crystal data for *Pf*FKBD35-D44 complex at the National Synchrotron Radiation Research Center (NSRRC) beamline 13B1. The NSRRC is a national user facility supported by the National Science Council of Taiwan, ROC; the Synchrotron Radiation Protein Crystallography Facility at NSRRC is supported by the National Research Program for Genomic Medicine. The authors also like to thank Dr. Aissatou Toure, Head of Pasteur Institute of Dakar, Senegal for providing the necessary support for testing on Clinical isolate cultures. We also thank our colleagues Chin Hui Li Christina and Babacar Diouf for their help in maintaining the cancer cell lines and clinical isolate cell line respectively. The authors also thank Dr. Karthigayan Guanalan assistance in performing the malarial growth inhibition studies. This study was supported by Singapore Ministry of Health IRG Grant NMRC/1245/2010.

Author contributions

A.H., M.N., S.R., P.R.P., H.S.Y., designed the experiments, A.H., M.N., S.R., prepared samples, performed the experiments and prepared figures, A.H., M.N., S.R., P.R.P., H.S.Y., wrote the manuscript, A.H., M.N., S.R., P.R.P., H.S.Y., analyzed and interpreted data. All authors reviewed the manuscript.

Additional information

Supplementary information accompanies this paper at http://www.nature.com/scientificreports

Competing financial interests: The authors declare no competing financial interests.

How to cite this article: Harikishore, A., Niang, M., Rajan, S., Preiser, P.R. & Yoon, H.S. Small molecule *Plasmodium* FKBP35 inhibitor as a potential antimalaria agent. *Sci. Rep.* **3**, 2501; DOI:10.1038/srep02501 (2013).